Plasma Sci. Technol. **19** (2017) 125504 (8pp) https://doi.org/10.1088/2058-6272/aa8806

Optical properties of titanium oxide films obtained by cathodic arc plasma deposition

Vukoman JOKANOVIĆ[1,2], Božana ČOLOVIĆ[1], Anka TRAJKOVSKA PETKOSKA[3], Ana MRAKOVIĆ[1], Bojan JOKANOVIĆ[4], Miloš NENADOVIĆ[1], Manuela FERRARA[5] and Ilija NASOV[6]

[1] Vinča Institute of Nuclear Sciences, University of Belgrade, Mike Petrovića Alasa 12-14, 11001 Belgrade, Serbia
[2] ALBOS Doo, Orahovačka 19, 11000 Belgrade, Serbia
[3] University St Kliment Ohridski, Faculty of Technology and Technical Sciences, Veles, R. Macedonia
[4] GL group, Werner-von-Siemens-Straβe, 86405 Metingen, Germany
[5] TE-STT-SCIS, Laboratorio Sviluppo Componenti ed Impianti Solari, Piazzale Enrico Fermi 1, 80055 Portici (NA), Italia
[6] Plasma Doo, 29 November 66/9, 1000 Skopje, R. Macedonia

E-mail: vukoman@vinca.rs

Received 6 July 2017, revised 21 August 2017
Accepted for publication 23 August 2017
Published 23 October 2017

Abstract

Structural and optical properties of nanometric titanium oxide (Ti_xO_y) films obtained by cathodic arc plasma deposition were investigated. Phase analysis by x-ray diffraction and Fourier-transform infrared spectroscopy showed the presence of anatase, rutile, Ti_2O_3, Ti_4O_7 and amorphous phases. Scanning electron microscopy images showed well-developed surface morphology with nano-patterns. Spectroscopic ellipsometry revealed film thicknesses of 53 and 50 nm, variable refractive indices dependent on the light wavelength and close to zero extinction coefficients for wavelengths higher than 500 nm. On the basis of ultraviolet–visible spectroscopy data and using the Tauc equation, band gap values for direct and indirect electron transitions were determined.

Keywords: optical materials, plasma deposition, thin films, ellipsometry

(Some figures may appear in colour only in the online journal)

1. Introduction

Cathodic arc plasma deposition (CAPD) is a powerful deposition technique, since cathodic arc plasmas are completely ionized with high energy ions, enhancing adhesion and formation of high density films [1–3]. It is mainly used for deposition of nitride and some oxide coatings, but also for deposition of multilayer coatings [2, 3] for various applications, like wear-resistant coatings on various tools and machines, decorative and corrosion resistant coatings on various house appliances, protective coatings against electromagnetic and radiofrequency interference, etc [4, 5].

Titanium dioxide (TiO_2) shows high refractive index, transparency in the visible region, excellent wear resistance and stability, high dielectric constant, semiconductor properties and it is chemically stable, thus it can be used for optical coatings, microelectronic devices and protective layers [6, 7]. Also, it shows ultra-hydrophilicity and stain resistance due to which its films are used as side-view mirrors in cars, deodorization which enables its application in air cleaners by deposition of the films onto filters, tents, tiles and sound barriers to provide their antifouling and antimicrobial functions [8, 9]. Crystalline TiO_2 thin films can be used for photocatalytic purification and solar energy conversion and also have good blood compatibility [10–12]. TiO_2 layers with amorphous phase can be used as high refractive layers in optical multilayer coatings, low-E systems or filters [13]. Their hydrophobic forms can be used to coat medical materials which are in contact with blood (like artificial heart valves, vascular stents, blood pressure sensors, etc), and thus to minimize the adsorption of blood proteins to their surface and to reduce the possibility of blood coagulation and further

thrombosis [12, 14]. TiO_2 coating produced by CAPD under UV light illumination also possesses significant antimicrobial properties, which are important for protection from medical device-associated infections [9, 15]. It is also an attractive alternative for the deposition procedure of such coatings as it allows rapid deposition of TiO_2 thin films in a mass production ready process with a high level of control of the coating microstructure and excellent adhesion to the substrate [16, 17].

The films obtained in this study consist of various titanium oxide phases: semi-conductive (Ti_2O_3 and Ti_4O_7) and dielectric (rutile, anatase and amorphous TiO_2), which give specific optical properties influenced by a parabolic decrease of refractive index values with wavelength. Also, the material shows close to zero extinction coefficients for wavelengths higher than 500 nm. Such low values of extinction coefficients indicate that this material may have potential to be applied as a laser, because after low energy excitation all conditions for the inverse electron occupation characteristic for spontaneous and subsequent stimulated emission are fulfilled.

2. Materials and methods

Ti_xO_y thin films were deposited on glass slides ($2.5 \times 5\,cm^2$) by CAPD. Prior to sputtering deposition the substrate surface was prepared by ion cleaning. Working conditions were: working vacuum -4×10^{-4} mbar, pressure of O_2- 2×10^{-1} bar, trigger voltage of pulsed arc -10 kV, pressure of Ar- 4×10^{-1} mbar, total working vacuum -1.8×10^{-3} mbar and current of arc evaporator -180 A.

After the deposition, one sample was analyzed without additional thermal treatment (sample 1) and the other sample was further thermally treated at 400 °C for 1 h (sample 2).

Phase composition of the samples was analyzed by x-ray diffraction (XRD; Philips PW 1050 powder diffractometer using Ni-filtered Cu-K_λ radiation) and Fourier-transform infrared spectroscopy (FTIR; Nicolet IS 50 FT-IR Spectrometer) methods. Optical properties were analyzed by ultraviolet–visible (UV–vis) spectroscopy. Microstructure analysis of the thin films was performed by scanning electron microscopy (SEM; JEOL JSM-6460).

Spectroscopic ellipsometry analysis of the samples was made using a J A Woollam variable angle spectroscopic ellipsometer (Model VB-400) and the optical parameters were estimated by the ellipsometric analysis program WVASE32. For each sample the ellipsometric analysis was performed to: 300–2500 nm and 50, 60, 70 degrees.

3. Results and discussion

3.1. XRD analysis

XRD patterns of the films obtained by CAPD (typical appearance of the films shown in appendix A) showed the presence of various Ti_xO_y phases: anatase, rutile, Ti_2O_3 and Ti_4O_7 (figure 1(a)). The sample without additional thermal treatment (sample 1) showed characteristic plane (101) for anatase at 25.55°, for rutile (110) at 27.38°, for Ti_2O_3 (012) at 23.65° and for Ti_4O_7 (−104) at 31.59°. The sample treated at 400 °C (sample 2) showed characteristic plane (101) for anatase at 25.84°, for rutile (110) at 27.47°, for Ti_2O_3 (012) at 23.83° and for Ti_4O_7 (−104) at 31.79°. These peaks are more clearly visible in figure 1(b) which represents a magnified part of figure 1(a). Beside these crystal phases, a TiO_2 amorphous phase with shifted stoichiometry is present as a dominant phase.

3.2. FTIR analysis

FTIR spectra of Ti_xO_y films confirmed the XRD findings (figures 2(a) and (b)). The bands between 1071 and 1022 cm^{-1} can be attributed to the ν(C–O) vibration, belonging to CO^{2-} adsorbed on the titanium surface. The bands at 880–896 cm^{-1} can be assigned to vibrations of the TiO_6 octahedron, related to Ti–O stretching bonds either directed to the interlayer space or to the outer surface formed nanotube. The bands at 765–751 cm^{-1} correspond to Ti=O bond vibration of Ti-suboxides shifted slightly towards smaller wavenumbers, due to lower content of oxygen and small grain sizes of suboxide nanoparticles. The bands around 657 cm^{-1} can be attributed to the TiO_6 octahedron, related to Ti–O stretching bonds, corresponding to rutile phase. The bands at 657–614 cm^{-1} correspond to O–Ti–O bonding in anatase morphology; this peak can also be assigned to surface phonon splitting of the vibration corresponding to peak at 657 cm^{-1} due to the small particle size of either anatase or rutile phase. The bands at 604–614 cm^{-1} show the presence of Ti–O and Ti–O–Ti stretching vibrations. The bands at 498–486 cm^{-1} probably correspond to the presence of suboxide phases Ti_2O_3 and Ti_4O_7. The peaks around 472 cm^{-1} correspond to O–Ti–O bonding in anatase morphology but they also can indicate the presence of Ti_2O_3 or Ti_4O_7 phases. The peaks between 464 and 452 cm^{-1} can be assigned to vibrations of the TiO_6 octahedron, related to Ti-O stretching bonds either directed to the interlayer space or to the outer surface formed nanotube, while the 448–449 cm^{-1} bands correspond to the phonon frequency of rutile phase. The bands between 441 and 433 cm^{-1} correspond to the phonon bands of nanocrystaline TiO_2 phase, while the bands at 429–406 cm^{-1} can be assigned either to anatase or rutile phase.

3.3. SEM investigations

SEM micrographs showed no significant differences between the samples (figure 3). Individual particles of irregular shape can be observed on the film surface with sizes from 50 to 110 nm. These particles on the film surface make typical nano-patterns indicating their possible application in photocatalysis (they have well-developed surface morphology) while from the aspect of optical properties they influence increased light scattering. Besides increased light scattering, the transmittance of the samples is satisfying (maximal transmittance of sample 1 is 41.2% and that of sample 2 is 63.9%, see section 3.5), which means that they can be applied in optical devices.

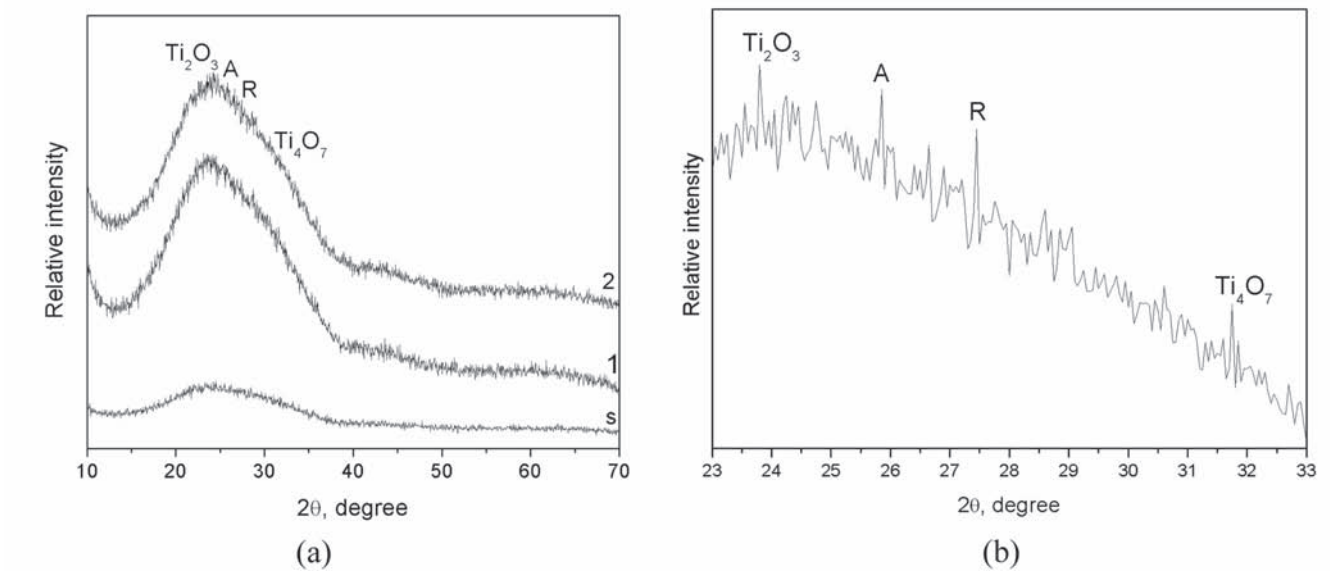

Figure 1. (a) XRD patterns of Ti_xO_y films obtained by CAPD (s-substrate, 1-sample 1, 2-sample 2, A-anatase, R-rutile). (b) Magnification of 23–33° region for sample 2.

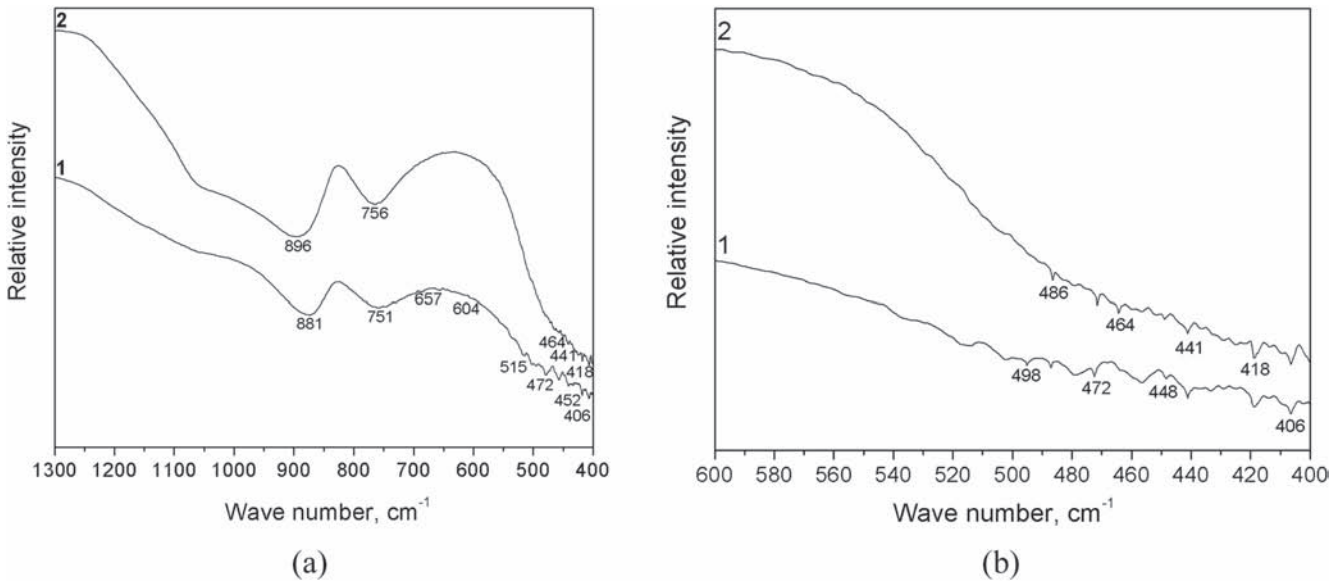

Figure 2. (a) FTIR spectra of Ti_xO_y films obtained by CAPD (1-sample 1, 2-sample 2). (b) Magnification of a 600–400 cm^{-1} region.

3.4. Refractive index and film thickness

Based on spectroscopy ellipsometry data, using software package WVASE32, an appropriate model has been created consisting of two layers, one layer of TiO_2 and one interlayer between the TiO_2 layer and glass substrate consisting of dominant TiO_2 and small amounts of Ti_2O_3 and Ti_4O_7 phases (see appendix B). The dependences of the refractive index and extinction coefficient of the wavelength for the TiO_2 thin film for sample 1 and sample 2 are shown in figures 4(a) and (b) respectively.

A significant decrease of the refractive index with wavelengths in the range 300–600 nm and slight decrease for longer wavelengths can be noticed in figure 4. The decrease of refractive index is high (about 0.9) in the narrow wavelength range (300–600 nm) in comparison to some values found in the literature where it decreases by about 0.1 in the range 400–1000 nm [18] or from 0.2–0.5 in the range 300–800 nm depending on annealing temperature [19, 20]. Similar behavior was found in TiO_2 film annealed at 800 °C where the refractive index rapidly decreased from 3.4 to 2.25 for wavelengths from 400 to 550 nm [20].

The stronger decrease of refractive index in comparison to values found in the literature is probably caused by the higher number of very small voids inside the films,

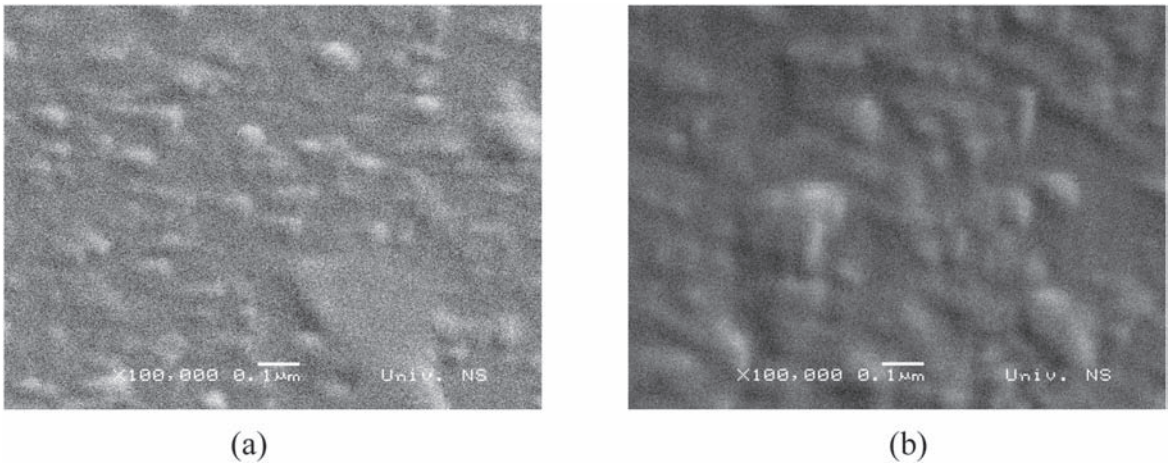

Figure 3. (a) SEM micrograph of sample 1. (b) SEM micrograph of sample 2.

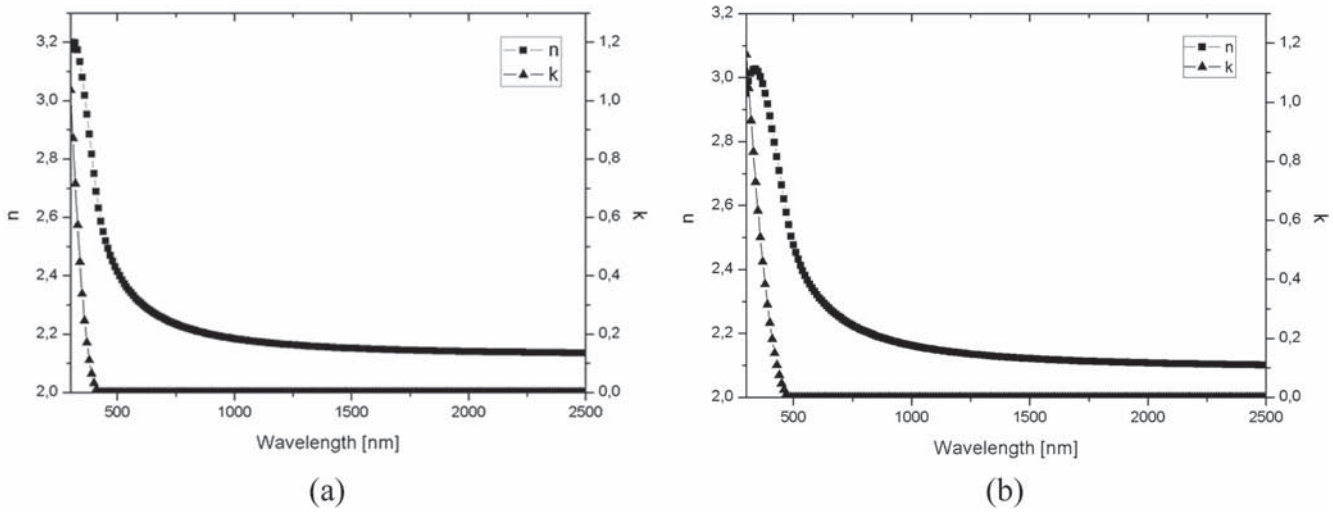

Figure 4. (a) Refractive index (n) and extinction coefficient (k) versus wavelength of the TiO_2 layer of sample 1. (b) Refractive index (n) and extinction coefficient (k) versus wavelength of the TiO_2 layer of sample 2.

particularly oxygen vacancies (induced by the slightly increased rate of film deposition), which induce increased dissipation of the incident light beam.

The extinction coefficients decreased with wavelength increase, reaching less than 0.01 at 500 nm and higher wavelengths. A similar behavior was noticed for TiO_2 film deposited on quartz glass at 300 °C [20], where extinction coefficient increased from 0.01 to 0.035 in the wavelength range 400–900 nm. Low values of extinction coefficients (also induced by the increased number of very small voids in the film volume) indicate that during low energy excitation, inverse electron occupation will occur (higher number of electrons in an excited state than in ground state) within this system, which leads to spontaneous and subsequent stimulated emission, for wavelengths higher than 500 nm. The low value of k indicates that the thin films possess good optical qualities especially for laser applications.

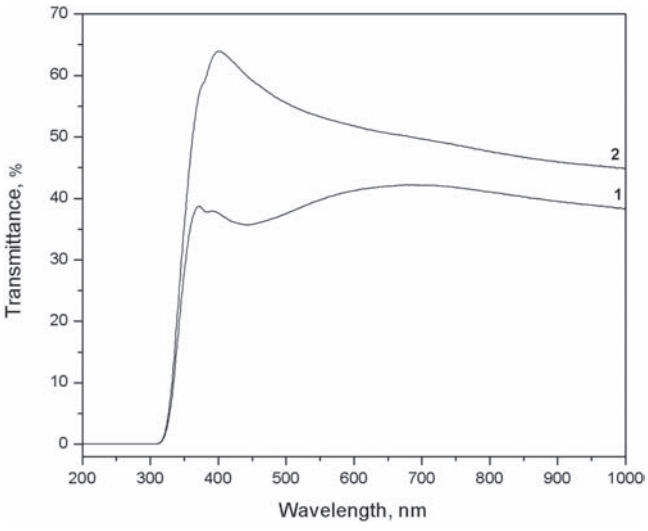

Figure 5. Transmittance of Ti_xO_y films obtained by CAPD.

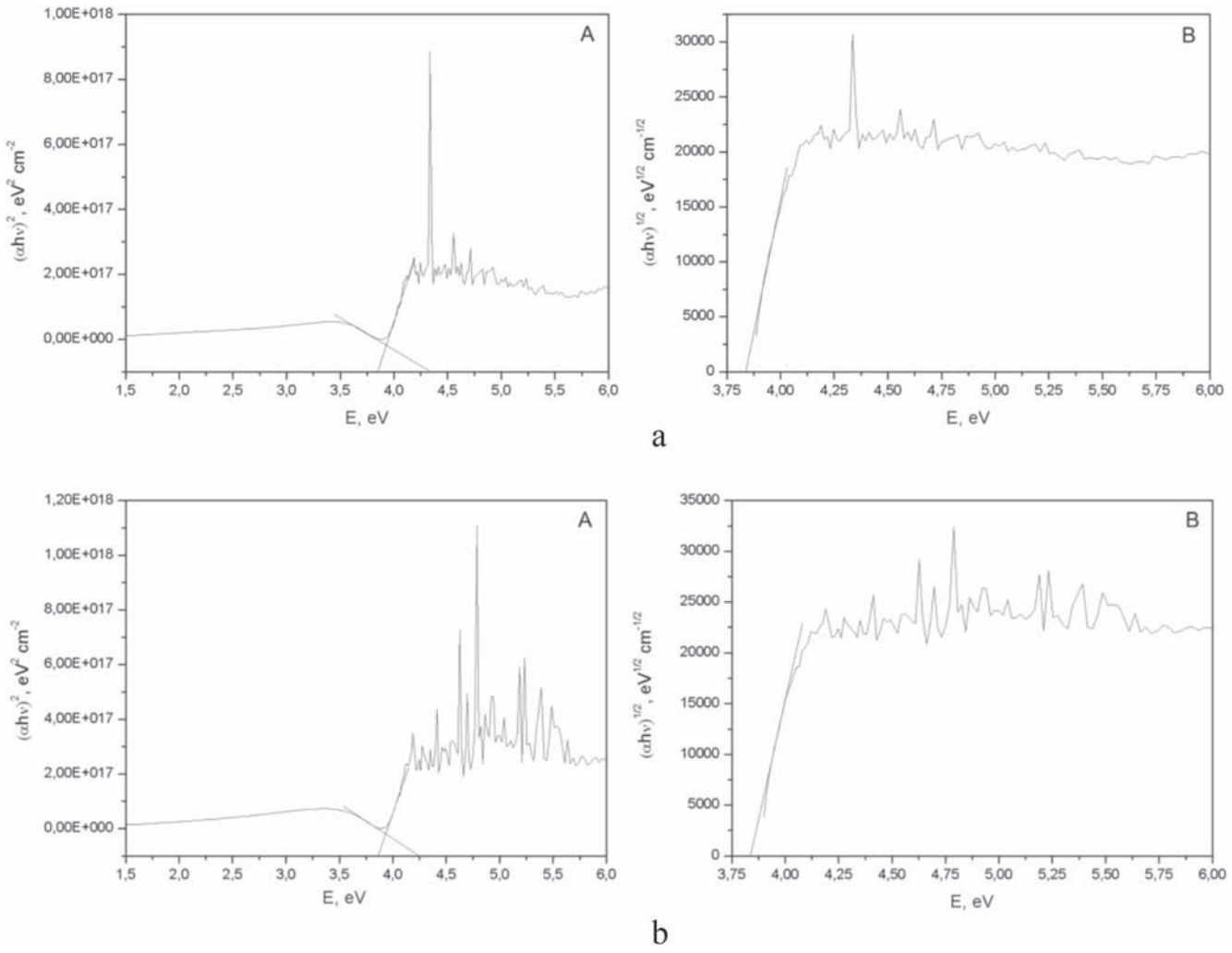

Figure 6. (a) Absorption coefficient dependence on the photon energy for sample 1 (A, B—direct and indirect transition, respectively). (b) Absorption coefficient dependence on the photon energy for sample 2 (A, B—direct and indirect transition, respectively).

The Ti_xO_y film thickness was calculated to be about 53 nm for sample 1, and about 50 nm for sample 2, while interlayer thickness was calculated to be a few nanometers for both samples.

3.5. UV–vis spectroscopy and band gap energy

Transmittance of Ti_xO_y films obtained by CAPD (figure 5) is close to zero for wavelengths less than 310 nm and then it increases rapidly. Sample 1 showed a maximum value of 41.2% for a wavelength of 690 nm, while the corresponding value for sample 2 was 63.9% for a wavelength of 400 nm (figure 5).

The optical band energy gaps of the Ti_xO_y films were estimated from the absorption coefficients of the films, calculated from their transmittance T and thickness d (obtained by ellipsometry) by [21]:

$$\alpha = -1/d \ln(T). \quad (1)$$

If a parabolic energy distribution of the density states for the valence and conduction bands is assumed, the E_g of titanium oxide film can be obtained from the plot of function $(\alpha h\nu)^{2/a}$ versus $h\nu$, derived from the Tauc equation:

$$\alpha(h\nu) = C(h\nu - E_g)^{a/2}/h\nu, \quad (2)$$

where E_g is the band gap of given material, C is constant, $a = 1$ for direct transition between edges of the valence and conduction bands, and $a = 4$ for indirect transition. The values of energy gaps were obtained by extrapolation of the linear part of plots (figure 6) [21].

For sample 1, the obtained values for direct transition were 3.85 eV for $\lambda = 285$–313 nm and 4.32 eV for $\lambda = 323$–346 nm, and for indirect transition 3.84 eV for $\lambda = 311$–317 nm (figure 6(a)). Sample 2 showed direct transitions at 3.86 eV for $\lambda = 304$–314 nm and 4.25 eV for $\lambda = 320$–340 nm, and indirect transition at 3.83 eV for $\lambda = 310$–318 nm (figure 6(b)). These band gap values for indirect or direct transitions corresponding to transitions inside the valence band and between valence and conductive

bands, and the band splitting inside of the crystal field, are induced by the presence of oxygen vacancies and corresponding distortion of the crystal lattice in the vicinity of Ti ions.

Accordingly, XRD investigation revealed different oxidative states of titanium: Ti^{3+} (Ti_2O_3), mixed Ti^{4+} and Ti^{3+} in ratio 1:1 (Ti_4O_7, first member of Magnéli phases) and Ti^{4+} (anatase, rutile). In all Ti_xO_y, titanium is in octahedral coordination, surrounded by six oxygen atoms, while each oxygen atom is surrounded by three titanium atoms [22]. Due to specific symmetry sites of titanium and oxygen atoms in each of these phases, the distortion of molecular orbitals occurs. This induces the splitting of Ti d orbitals into a triply degenerated t_{2g} band which consists of d_{xy}, d_{xz} and d_{yz} orbitals (higher energy state) and doubly degenerated e_g band which consists of $d_{x^2-y^2}$ and d_{z^2} orbitals (lower energy state). The t_{2g} band splits at least into two components due to different types of octahedral distortions (rutile—tetragonal distortion, Ti_2O_3—trigonal distortion, Ti_4O_7—orthorhombic-like distortion).

This splitting of the t_{2g} orbitals in the valence band (near the Fermi level) influences different intra-band transitions and corresponding band gaps, during interaction with the incident light wave. Taking into account that in TiO_x ($x < 2$), three groups of bands can be found near the Fermi level: −0.4 to 2.4 eV (Ti 3d t_{2g}), and 2.4 to 4.1 eV (Ti 3d $e_g{}^{\sigma}$), while Ti 4 s bands correspond to energies higher than 3.55 eV [23], the dominant partition of the (Ti 3d $e_g{}^{\sigma}$) transitions is obvious, regardless of which kind of transitions (direct or indirect) is observed, showing that transitions from a deeper electronic states inside the valence and conductive bands are prevailing. This is typical for oxygen vacancy poor systems, because in this state the interactions between Ti and O are stronger, inducing higher values of the gaps between lowest unoccupied molecular orbital (LUMO) levels (low unoccupied Ti 3d orbitals) and highest occupied molecular orbital (HOMO) levels, corresponding to the valence band of O 2p orbitals.

4. Conclusions

Nanometric Ti_xO_y films obtained by cathodic arc plasma deposition consisted predominantly of amorphous TiO_2 phase, with the presence of anatase, rutile, Ti_2O_3 and Ti_4O_7 phases. The films with thicknesses about 50 nm showed surface roughness with characteristic nano-patterns. Their refractive indices varied with the light wavelength, showing a parabolic decrease. The extinction coefficients decreased with wavelength increase, reaching less than 0.01 at 500 nm and higher wavelengths. The extinction coefficients showed an almost linear decrease to near zero value, indicating that this system can be potentially applied as a laser for red and infrared areas.

Acknowledgments

Financial support for this work was provided by the Ministry of Education, Science and Technological Development of the Republic of Serbia (grant 172026) and COST action MP1306.

Appendix A. Appearance of the films

Typical appearance of the Ti_xO_y films obtained by CAPD is shown in figure A1.

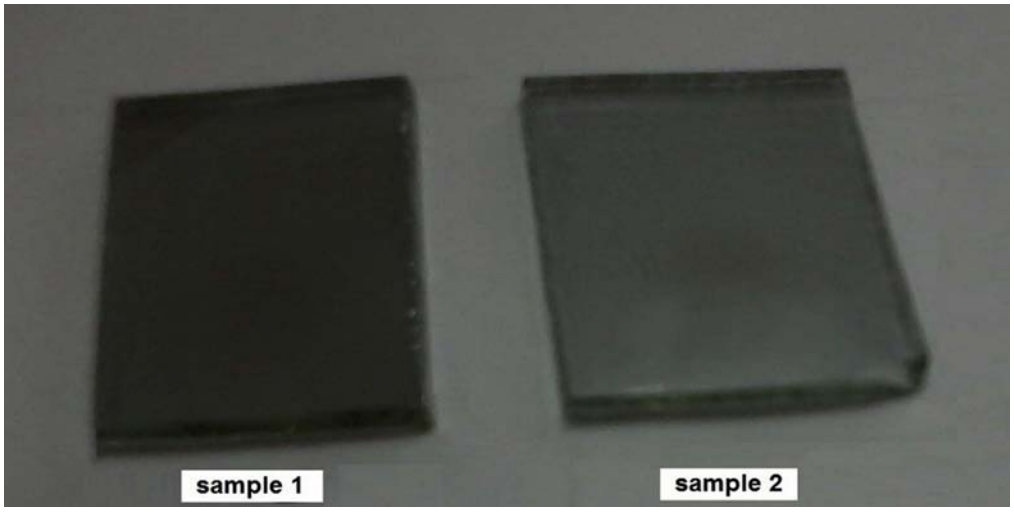

Figure A1. Typical appearance of the Ti_xO_y films obtained by CAPD.

Appendix B. Fitting procedure of the ellipsometric data

Spectroscopic ellipsometry measures changes in the polarization state (expressed as psi, Ψ, and delta, Δ) of a light beam reflected on a sample surface. Further data analysis consisting of the modeling of the layer structure and curve fitting enables extraction of the information on film refractive index n, extinction coefficient k and film thickness.

After the ellipsometric data were acquired, in the range 300–2500 nm, a fitting procedure to calculate the optical parameters and thickness was used to minimize the mean square error (*MSE*), given by:

$$MSE = \sqrt{\frac{1}{2N-M}\sum_{i=1}^{N}\left[\left(\frac{\psi_i^{\mathrm{mod}}-\psi_i^{\mathrm{exp}}}{\sigma_{\psi,i}^{\mathrm{exp}}}\right)^2+\left(\frac{\Delta_i^{\mathrm{mod}}-\Delta_i^{\mathrm{exp}}}{\sigma_{\Delta,i}^{\mathrm{exp}}}\right)^2\right]},$$

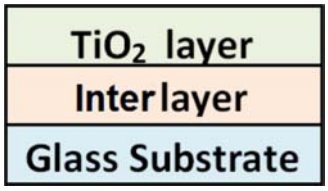

Figure B1. Model used to fit data for sample 1 and sample 2.

where N is the number of (Ψ, Δ) pairs, M is the number of variable parameters in the model and σ are the standard deviations on the experimental data points.

For interpretation of the ellipsometric data it was necessary to create an appropriate model. Typical models used for data fitting consist of substrate/layer 1/…/layer N. In this case for both samples a two-layer model was carried out: one homogeneous layer of TiO_2 and one interlayer of several nanometers between the TiO_2 layer and glass substrate consisting of dominant TiO_2 and small amounts of Ti_2O_3 and Ti_4O_7 phases, as reported in figure B1.

For each layer different oscillators were used. The properties of the titanium oxide layer were described using a Tauc–Lorentz oscillator [24]. This model is used to describe the dielectric function of many amorphous materials. To describe the properties of the interlayer a Gaussian oscillator [25], Drude oscillator [26] and Lorentz oscillator [27] were used. For each sample the generated and experimental data were compared, reported in figure B2, and the perfect match of these data confirms the high accuracy of ellipsometric estimation.

The good agreement of experimental and generated data shows that a correlation between refractive index and thickness is well controlled.

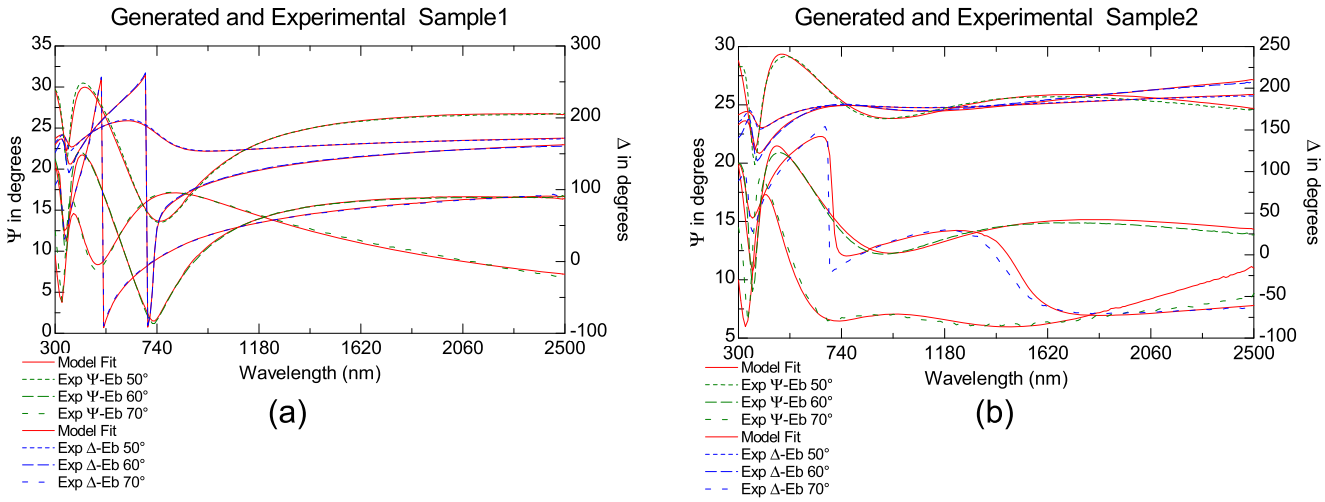

Figure B2. (a) Generated and experimental data for sample 1. (b) Generated and experimental data for sample 2.

References

[1] Bendavid A and Martin P J 2014 *J. Aust. Ceram. Soc.* **50** 86 (https://www.researchgate.net/publication/261762263_Review_of_thin_film_materials_deposition_by_the_filtered_cathodic_vacuum_arc_process_at_CSIRO)
[2] Martin P J, Bendavid A and Kinder T J 1996 *Surf. Coat. Technol.* **81** 36
[3] Shi Z B *et al* 2004 *Plasma Sci. Technol.* **6** 2581
[4] Razvan I *et al* 2014 *Key Eng. Mat.* **614** 206
[5] Vereshchaka A A *et al* 2014 *Int. J. Adv. Manuf. Technol.* **72** 303
[6] Bedikyan L, Zakhariev S and Zakharieva M 2013 *J. Chem. Technol. Metall.* **48** 555 (http://dl.uctm.edu/journal/node/j2013-6/2-Bedikyan_p-555-558.pdf)
[7] Rathee D, Arya S K and Kumar M 2011 *Front. Optoelectron. China* **4** 349
[8] Wang R *et al* 1997 *Nature* **388** 431
[9] Romero L *et al* 2015 *Chem. Vap. Deposition* **21** 63
[10] Kleiman A *et al* 2011 *Appl. Catal.* B **101** 676
[11] Carp O, Huisman C L and Reller A 2004 *Prog. Solid State Chem.* **32** 33
[12] Maitz M F *et al* 2003 *J. Biomater. Appl.* **17** 303
[13] Chang C C *et al* 2010 *J. Sol-Gel Sci. Technol.* **55** 199
[14] Bakir M 2012 *J. Biomater. Appl.* **27** 3
[15] Visai L *et al* 2011 *Int. J. Artif. Organs* **34** 929
[16] Takikawa *et al* 1999 *Thin Solid Films* **348** 145
[17] Kleiman A, Márquez A and Lamas D G 2007 *Surf. Coat. Technol.* **201** 6358
[18] Mergel D *et al* 2000 *Thin Solid Films* **371** 218
[19] Hou Y Q *et al* 2003 *Appl. Surf. Sci.* **218** 98
[20] Won D J *et al* 2001 *Appl. Phys.* A **73** 595
[21] Karasiński P *et al* 2012 *J. Sol-Gel Sci. Technol.* **61** 355
[22] Stoyanov E, Langenhorst F and Steinle-Neumann G 2007 *Am. Mineral.* **92** 577
[23] Eyert V, Schwingenschlögl U and Eckern U 2005 *Europhys. Lett.* **70** 782
[24] Jellison G E Jr and Modine F A 1996 *Appl. Phys. Lett.* **69** 371
[25] De Sousa Meneses D, Malki M and Echegut P 2006 *J. Non-Cryst. Solids* **351** 769
[26] Tiwalda T E *et al* 1998 *Thin Solid Films* **313–314** 661
[27] Wooten F 1972 *Optical Properties of Solids* (New York: Academic Press) p 52 (http://www.phys.ufl.edu/~tanner/Wooten-OpticalPropertiesOfSolids-2up.pdf)